Accepted Manuscript

Bright luminescence of Gd^{3+} sensitized RE^{3+}-doped SiO_2-$BaGdF_5$ glass-ceramics for UV-LEDs colour conversion

A.C. Yanes, J. del-Castillo

PII: S0925-8388(16)33777-X

DOI: 10.1016/j.jallcom.2016.11.296

Reference: JALCOM 39793

To appear in: *Journal of Alloys and Compounds*

Received Date: 27 July 2016

Revised Date: 19 November 2016

Accepted Date: 21 November 2016

Please cite this article as: A.C. Yanes, J. del-Castillo, Bright luminescence of Gd^{3+} sensitized RE^{3+}-doped SiO_2-$BaGdF_5$ glass-ceramics for UV-LEDs colour conversion, *Journal of Alloys and Compounds* (2016), doi: 10.1016/j.jallcom.2016.11.296.

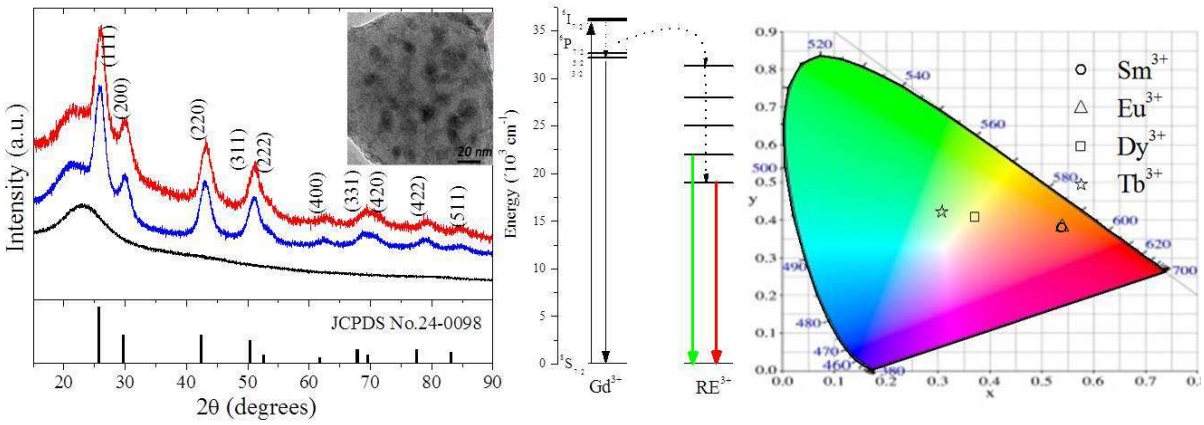

Bright luminescence of Gd^{3+} sensitized RE^{3+}-doped SiO_2-$BaGdF_5$ glass-ceramics for UV-LEDs colour conversion

A. C. Yanes, J. del-Castillo*

Departamento de Física, Universidad de La Laguna, 38206 La Laguna, Spain

Abstract

RE-doped (Eu^{3+}, Sm^{3+}, Dy^{3+} or Tb^{3+}) nano-glass-ceramics containing $BaGdF_5$ nanocrystals, have been successfully obtained under thermal treatment of precursor sol-gel glasses. X-ray diffraction, high-resolution transmission electron microscope images and energy dispersive X-ray spectroscopy measurements confirmed the precipitation and distribution of cubic $BaGdF_5$ nanocrystals (around 10 nm in size) in the glass matrix. The luminescent properties, via excitation and emission spectra along with decay curves, were studied. In order to complete the structural analysis, the luminescent features of Eu^{3+} and Sm^{3+} ions were also used as sensitive probes, confirming the distribution of a significant fraction of dopant ions into the fluoride nanocrystalline environment. Intense visible emissions were obtained through efficient energy transfer from Gd^{3+} to RE ions, which leads to consider these materials as potential emitting phosphors for colour converted UV LEDs.

Keywords: Nano-Glass-Ceramics, Rare-Earth Ions, Sol–Gel Technique, Energy Transfer.

Corresponding author: fjvargas@ull.edu.es

1. Introduction

Nano-materials doped with rare-earth (RE) ions are an important class of materials, for they present a broad range of applications, such as temperature sensors, solid-state lasers, optical amplifiers, lighting and displays, solar cells, labelling, and so on [1-7]. In particular, RE-doped oxyfluoride nano-glass-ceramics (nGCs) are currently being extensively investigated as blue or UV converting white light emitting diodes wLEDs in order to replace the traditional phosphors powder and organic resins, respectively [4,8-15]. This type of materials preserves the mechanical, thermal and chemical properties of oxide glass and shows the low phonon energy of fluoride environments that prevents non-radiative multiphoton relaxations [8,16]. Moreover, nGCs present a high degree of transparency due to the much smaller size of nanocrystals (NCs) being dispersed in a transparent matrix (e.g. silica), which is very important for their practical applications. In this regard, RE doped-oxifluoride nGCs containing Y and La based (with similar ionic radii and valence) NCs have been widely investigated [2, 9, 17-24] due to the easy and homogeneous incorporation of RE ions into the fluoride nanocrystalline phase, which enhances the photoluminescence efficiency. In particular, in nGCs containing Tm^{3+}-Yb^{3+} co-doped YF_3 NCs [2] and Er^{3+}-Tb^{3+}-Yb^{3+} co-doped Ba_2LaF_7 NCs [17], up-conversion emissions were studied by D. Chen et al and H. K. Dan et al, respectively. Moreover, authors have confirmed the distribution of a significant fraction of Eu^{3+} and Sm^{3+} ions into $BaYF_5$ nanocrystalline environment, with sizes around 11 nm [18]. They have also studied the energy transfer (ET) mechanisms in Dy^{3+}-Tb^{3+} [19], Ce^{3+}-Tb^{3+} [20] and Sm^{3+}-Eu^{3+} [21] under near UV-excitation, in nGCs comprising YF_3, KYF_4 and LaF_3 NCs, respectively, and obtained white light emission in nGCs with Ce^{3+}-Tb^{3+}-Eu^{3+} co-doped KYF_4 NCs, through ET processes [22]. Additionally, white light was also observed in Eu^{2+}-Eu^{3+} co-doped LaF_3 based nGCs under UV excitation by S.H. Lee et al [9], and in nGCs comprising Yb^{3+}-Er^{3+} co-doped $LiYF_4$ NCs and Yb^{3+}-Ho^{3+}-Tm^{3+}-Ce^{3+} co-doped YF_3 NCs, under IR excitation, by M. Secu et al [23] and D. Chen et al [24] respectively.

Among the RE ions, Eu^{3+}, Sm^{3+}, Tb^{3+} and Dy^{3+} are being used in the development of wLEDs due to their bright visible emissions [22, 25-27]. Even though these ions exhibit high luminescence quantum efficiencies when they are located in low phonon energy environments, they also present the disadvantage of having a low absorption strength for

the 4f-4f transitions in the UV to blue region. Thus, in principle, it seems that these ions are not suitable to be used in LED conversion phosphors. However, this problem could be solved by incorporating RE ions to Gd^{3+}-based fluoride NCs acting as low phonon energy hosts (like those based on La^{3+} and Y^{3+}), but at the same time, as sensitizers for RE ions. Thus, compared with other fluorides, $BaGdF_5$ (phonon energy of 457 cm^{-1} [28]) is considered an excellent host matrix for down and up-conversion processes. As reported in [29] the up-conversion luminescence intensity of active-core/active-shell ($BaGdF_5$:Yb^{3+}-Er^{3+}/$BaGdF_5$:Yb^{3+}) nanoparticles was much higher than that of β-$NaYF_4$:Yb^{3+}-Er^{3+} nanoparticles with similar particle size and the same doping concentration. Moreover, ET from Gd^{3+} to RE ions, has been observed and studied by many researchers [27, 30-33]. In these cases, Gd^{3+} ions can efficiently absorb UV radiation and then transfer energy to the RE ions.

On the other hand, there are only a few reports about photo-luminescent properties of gadolinium fluoride based nGCs, where most of them have been prepared by a melt-quenching method [8, 10, 33-38]. In this respect, a different method to obtain nGCs is by thermal treatment of precursor glasses synthesised by a sol-gel technique. This method presents advantages such as its simplicity, low cost and precise control of the final composition [39] when compared with conventional melting methods. Moreover, starting materials (in particular RE-dopant ions) can be mixed in the sol-gel method at a molecular level, thus improving the luminescence.

In this work, we present un-doped and RE-doped nGCs containing $BaGdF_5$ NCs obtained by a sol-gel method. The presence of cubic phase structure $BaGdF_5$ NCs was confirmed by X-ray diffraction (XRD) patterns and Transmission Electron Microscopy (TEM-HRTEM) images. In order to analyse the incorporation grade of the RE dopant ions in the $BaGdF_5$ NCs, Eu^{3+} and Sm^{3+} ions were also used as structural optical probes taken advantage of the hypersensitive nature of the $^5D_0 \rightarrow {}^7F_2$ and $^4G_{5/2} \rightarrow {}^6H_{9/2}$ transitions respectively, allowing us to distinguish between crystalline and glassy environments for RE ions. In all cases, an efficient ET between Gd^{3+} and RE ions (yielding intense visible emissions) was demonstrated, and the corresponding mechanisms were described.

2. Experimental

Silica glasses with composition $95SiO_2$-$5BaGd_{(1-x)}RE_xF_5$ (x= 0 or 0.02) in mol%, where RE = Eu^{3+}, Sm^{3+}, Dy^{3+} and Tb^{3+}, were obtained by sol-gel method in a similar way

as the one described in ref. [40]. The solution of tetraethoxysilane (TEOS, 99.999% Aldrich) $Si(OCH_2CH_3)_4$, used as a source of SiO_2 in ethanol and deionized H_2O with acetic acid (used as catalyst in the hydrolysis and polymerization reaction) was stirred for 1 h. The molar ratio of TEOS:ethanol:H_2O:CH_3COOH was 1:4:10:0.5. $Ba(CH_3COO)_2$ (99.999% Aldrich) and $Gd(CH_3COO)_3 \cdot xH_2O$ (99.9% Aldrich) were used as sources of Ba and Gd respectively. The required quantities of $Ba(CH_3COO)_2$, $Gd(CH_3COO)_3 \cdot xH_2O$, $Eu(CH_3COO)_3 \cdot xH_2O$ (99.9% Aldrich), $Sm(CH_3COO)_3 \cdot xH_2O$ (99.9% Aldrich), $Dy(CH_3COO)_3 \cdot xH_2O$ (99.9% Aldrich) and $Tb(CH_3COO)_3 \cdot xH_2O$ (99.9% Aldrich) were dissolved in a CF_3COOH and H_2O solution, and slowly mixed with the initial solution. The molar ratio of metal ions to CF_3COOH was 1:5. In order to make the solution homogeneous, it was stirred vigorously for 1 h at room temperature. A highly transparent gel was obtained by leaving the resulting homogeneous solution in a sealed container at 35 ºC for several days. The gels were then dried by slow evaporation for approximately four weeks to remove residual water and solvents. Finally, these sol-gel glasses were heat-treated in an air atmosphere at 650 ºC in order to achieve the controlled precipitation of $BaGdF_5$ NCs required to produce transparent nGCs.

Powder XRD patterns of the samples were recorded with a Philips Panalytical X'Pert Pro diffractometer equipped with a primary monochromator, a Cu $K_{\alpha 1,2}$ radiation source, and an X'Celerator detector. The XRD patterns were collected with a step of 0.016º in the 2θ angular range from 15-90º and an acquisition time of 2 h. Furthermore, the diffraction pattern of LaB_6 was used as an internal standard to calibrate the parameters of the instrumental profile. TEM-HRTEM images and energy dispersive X-ray spectroscopy (EDS) were obtained by using a JEOL 2010F microscope operating at 200 kV and equipped with a Field Emission Gun, which allowed us to achieve a point-to-point resolution of 0.19 nm. Samples were prepared by dispersing fine powder, obtained by grinding the samples in acetone and dropping them onto carbon-coated copper grids. Selected areas of the HRTEM images were mathematically filtered by means of Fast Fourier Transform (FFT) analysis, resulting in Power Spectra patterns, corresponding to the eigen-frequencies of the observed NCs. Furthermore, the relevant frequencies were selected in order to filter the noise in the zoomed areas of the HRTEM images and to produce higher contrast images of the atomic planes of the observed NCs. Moreover, the presence of $BaGdF_5$ in the nanocrystalline environment can be confirmed by EDS measurements.

Luminescence measurements were carried out by a PTI QuantaMaster spectrometer controlled by Felix32 software. For the steady state measurements, samples were excited with light from a 75 W Xe arc lamp whose beam was directed through a 0.2 m monochromator and detected with a 0.2 m monochromator with a R928 photomultiplier. For time-resolved photoluminescence measurements, a Xenon flash lamp was used as excitation source and the signal was detected with a digital storage system controlled by a PC. All spectra were collected at room temperature and corrected by the instrumental response.

3. Results and discussion

3.1 Structural characterization

Structural characterization has been carried out by XRD and TEM-HRTEM measurements. The XRD patterns of nGCs with composition $95SiO_2$-$5BaGdF_5$ un-doped and Eu^{3+}-doped, heat-treated at 650 ºC are shown in Fig.1 along with a precursor sol-gel glass.

For the precursor sol-gel glass, a broad diffraction band around 22º is observed, corresponding to amorphous SiO_2. However, for both nGCs, superposed to this broad band, diffraction peaks at 25.6, 29.7, 43.2, 51.0, 62.4, 69.3, 77.5 and 83.2º can be clearly observed, which can be related with the successful precipitation of $BaGdF_5$ cubic phase (JCPDS File Nº 24-0098, space group *Fm-3m* and cell parameter a=6.023Å) (see Fig.1). No second crystalline phase was detected, indicating a high degree of purity. By using the FullProf software [41], the experimentally calculated cell parameter for the un-doped nGC is 5.990 Å. This value is comparable with that obtained in RE-doped $BaGdF_5$ NCs with sizes around 10 nm (5.866 Å) [42] and with those corresponding to pure and RE-doped $BaGdF_5$ NCs (5.884 and 5.828 Å respectively) with sizes around 18 nm [43].

The XRD patterns of nGCs doped with Sm^{3+}, Dy^{3+} or Tb^{3+} (not shown), also present similar characteristics, i.e. location, relative intensity and broadness of the XRD peaks, pointing out that the RE doping level does not significantly affect the phase structure. By using the strongest peak at 2θ=25.6º and the Scherrer equation, the calculated mean NC size for the nGCs is around 10 nm, which is smaller than those obtained by K. Biswas et al [34] (around 12 nm), W. Zhang et al [8] (around 10-20 nm), P. Karmakar et al [44] (around 8-12 nm), Q. Wang et al [45] (around 13-28 nm) and S. Huang et at [35]

(around 18-27 nm), in $BaGdF_5$ nGCs. It is worth mentioning that all nGCs present a high degree of transparency due to the fact that precipitated NC sizes are smaller than the wavelength of the visible light.

Moreover, in order to confirm the presence of $BaGdF_5$ NCs in the Eu^{3+}-doped nGC, EDS spectra of the glassy matrix and an area containing glass matrix with several $BaGdF_5$ NCs are presented in Fig.2 (a) and (b), respectively. The EDS spectrum taken from the glass matrix only shows strong signals from Si and O elements (Cu and C peaks originating from the copper grid). However, intense Ba, Gd and F peaks are clearly detected in the EDS spectrum from the nanocrystalline domain. The atomic ratios of Ba/Gd/F are 1.08/1/4.65, which is in excellent agreement with the theoretical atomic Ba/Gd/F ratio of 1/1/5 in $BaGdF_5$, taking the accuracy of EDS spectroscopy into account.

In order to investigate the microstructure of the nGCs, TEM and HRTEM images were collected. Thus, TEM bright-field micrograph of Eu^{3+}-doped nGC, reveals a homogenous distribution of $BaGdF_5$ dark spherical nanocrystallites (with sizes around 10 nm) dispersed on the grey background in silica glassy matrix, which agrees with the estimate by the Scherrer equation in the XRD analysis (see Fig.3(a)). It is known that the nanocrystalline phase formation homogeneously distributed in the glassy matrix is a crucial aspect in the optical applications of nGCs [46]. Moreover, the corresponding HRTEM image shows few nanocrystalline domains, pointing out the detailed lattice structure of different $BaGdF_5$ NCs, squared in red and blue (see Fig.3(b)). In this sense, the left-top side inset in Fig.3(b) displays the power spectrum obtained from the squared NCs and direct images filtered by using the frequencies determined from the FFT pattern. The resolved lattice fringes (an indicator of their high degree of crystallinity) present a constant spacing of 3.37 and 3.01 Å that can be ascribed to (111) and (200) planes of cubic $BaGdF_5$, respectively.

3.2. Luminescence

We now focus on the spectroscopic study in terms of excitation and emission spectra, along with time-resolved measurements in $BaGdF_5$ nGCs un-doped and doped with Eu^{3+}, Sm^{3+}, Dy^{3+} and Tb^{3+} ions. These dopant ions have been selected due to their multicolored and bright luminescence, related with an efficient ET from Gd^{3+} ions, as will be discussed next.

Excitation and emission spectra of the un-doped nGC are shown in Fig.4, detecting and exciting at the indicated wavelengths. The energy level diagram of Gd^{3+} ions is also included. The excitation spectrum consists in sharp and structured peaks in the characteristic UV region of Gd^{3+} ions, assigned to transitions coming from the ground level $^8S_{7/2}$ to the excited levels. The corresponding emission spectrum, exciting at the most intense excitation peak at 272 nm, shows a unique emission peak located at 311 nm, which corresponds to the transition from the excited level ^6P_J to the ground level.

Given that the main absorption bands of different RE ions (such as Eu^{3+}, Sm^{3+}, Dy^{3+} and Tb^{3+}) overlap with the $^6P_J \rightarrow {}^8S_{7/2}$ emission of Gd^{3+} ions at 311 nm, the luminescence of these RE ions can be improved by using the Gd^{3+} ion as sensitizer, exciting at 272 nm, where the strongest excitation peak of Gd^{3+} ions is located.

In this sense, a luminescent study of Eu^{3+}-doped nGCs is carried out first, using Eu^{3+} ions as spectroscopic probe according to its energy level diagram (see Fig.5). The excitation spectrum detecting at 593 nm (corresponding to $^5D_0 \rightarrow {}^7F_1$ transition of Eu^{3+} ions) is shown in Fig.6(a). Sharp excitation peaks can be observed centred at 248, 272 and 307 nm, corresponding to transitions from the $^8S_{7/2}$ ground level to ^6D_J, ^6I_J and ^6P_J excited levels of Gd^{3+} ions respectively, suggesting the existence of ET from Gd^{3+} to Eu^{3+} ions. Besides, well-resolved characteristic peaks of Eu^{3+} above 350 nm can be assigned to transitions from the $^7F_0$ ground level to $^5D_4$, ^5G_J, $^5L_7$, $^5L_6$, $^5D_3$, $^5D_2$ and $^5D_1$ excited levels. It is clear that the excitation peaks assigned to Eu^{3+} ions are much weaker than the ones corresponding to Gd^{3+} ions, showing that the sensitization through Gd^{3+} ions is much more efficient than direct excitation of Eu^{3+} ions.

Fig.6(b) shows the corresponding emission spectra obtained by direct excitation of Eu^{3+} ions at 393 and 464 nm, and exciting through the Gd^{3+} ions at 272 nm. The spectrum obtained exciting at 393 nm ($^7F_0 \rightarrow {}^5L_6$), where all the Eu^{3+} ions located in the sample are excited, presents emissions coming from $^5D_1$ and $^5D_0$ excited levels, with narrow Stark components characteristic of Eu^{3+} ions in a crystalline host. These emissions are more intense (x35) and present a better resolved structure than the one obtained when exciting at 464 nm ($^7F_0 \rightarrow {}^5D_2$), which is a forbidden transition for Eu^{3+} ions in an environment with inversion symmetry, similar to the Eu^{3+} ions spectra in glassy hosts (see inset in Fig.6(b)). These results suggest that an important fraction of Eu^{3+} ions are distributed into the

centrosymmetric $BaGdF_5$ NCs, while the rest is distributed on their surfaces or remains in the glass phase.

The values obtained for the $^5D_0 \rightarrow {}^7F_2/{}^5D_0 \rightarrow {}^7F_1$ asymmetry ratio R (an indicator of how far the Eu^{3+} ion local environment is from being centrosymmetric [47]) are also in agreement with this interpretation. Thus, R values of 0.78 and 1.53 were obtained by exciting at 393 and 464 nm respectively.

On the other hand, the emission spectrum under indirect excitation at 272 nm (corresponding to the Gd^{3+} ions) presents, along with the $^6P_J \rightarrow {}^8S_{7/2}$ emission of Gd^{3+} ions at 311 nm, emission peaks corresponding to Eu^{3+} ions with the same features as the ones obtained by exciting at 393 nm, although much more intense (x 90). This fact indicates that the Eu^{3+} ions involved in these emissions should be incorporated into the $BaGdF_5$ NCs substituting the Gd^{3+} ions, further confirming that the excitation efficiency is much higher for the Eu^{3+} ions in the NCs by ET from the Gd^{3+} ions than by direct excitation.

We then study the luminescent properties in the Sm^{3+}-doped nGC according to the energy level diagram (see Fig.5). This also allows us to complete the structural analysis of these nGCs, for these ions (such as Eu^{3+} ions) have been frequently used to investigate the local symmetry around RE ions.

The excitation spectrum detecting at 597 nm (corresponding to $^4G_{5/2} \rightarrow {}^6H_{7/2}$ transition of Sm^{3+} ions) is shown in Fig.7(a). In the UV region, under 325 nm, several excitation peaks can be observed, corresponding to transitions from the $^8S_{7/2}$ ground level to the excited levels ^6D_J, ^6I_J and ^6P_J of Gd^{3+} ions. This shows the existence of ET processes from Gd^{3+} to Sm^{3+} ions. In addition, we can also observe excitation peaks from 350 nm ascribed to transitions from the $^6H_{5/2}$ ground level to $^4H_{7/2}$, $^4K_{13/2}$, $^4F_{7/2}$ and $^4I_{11/2}$ excited levels of Sm^{3+} ions, labelled in the magnified spectrum in Fig.7(a). Similarly to Eu^{3+}-doped nGCs, the excitation peaks assigned to Sm^{3+} ions are much weaker than the Gd^{3+} ones, revealing that the sensitization through these ions is much more efficient than by direct excitation of Sm^{3+} ions.

Fig.7(b) shows the emission spectra obtained by direct excitation of the Sm^{3+} ions at 398 nm and under indirect excitation (through the Gd^{3+} ions) at 272 nm. Spectra exciting at 398 and 272 nm present similar features, with four main emission peaks at 561, 597, 646 and 704 nm, coming from the $^4G_{5/2}$ excited level, although much more intense (x80) when exciting through the sensitizer, i.e. Gd^{3+} ions. Thus, taking into account that the transitions

$^4G_{5/2}\rightarrow{}^6H_{9/2}$ (at 646 nm) and $^4G_{5/2}\rightarrow{}^6H_{5/2}$ (at 561 nm) present ED and MD character, respectively, the asymmetry ratio R ($^4G_{5/2}\rightarrow{}^6H_{9/2}/{}^4G_{5/2}\rightarrow{}^6H_{5/2}$) also allows the use of Sm^{3+} ions as spectroscopic probe in order to characterize the local environment. In this sense, the emission spectrum of the SiO_2 glass doped with Sm^{3+} (see inset in Fig.7b) shows that the transition $^4G_{5/2}\rightarrow{}^6H_{9/2}$ is predominant, with an R value of 6.23, indicating the dominance of a non-inversion symmetry associated with a vitreous environment. On the other hand, the emission spectra exciting at 272 and 398 nm are shifted with respect to the glass one due to the crystal field effect. Moreover, they present lower R values of 2.75 and 2.86 respectively, which can be related with an inversion symmetry environment for Sm^{3+} ions in the $BaGdF_5$ NCs.

Then, once the incorporation of RE ions was confirmed, we studied the luminescent properties in nGCs doped with Tb^{3+} or Dy^{3+} ions, due to their interesting emissions in the visible range (see Fig. 8). Thus, Fig.8(a) shows excitation and emission spectra of Tb^{3+}-doped nGCs, detecting and exciting at the indicated wavelengths. The excitation spectrum detecting at 543 nm, corresponding to the most intense $^5D_4\rightarrow{}^7F_6$ transition of Tb^{3+} ions (see energy level diagram in Fig.5) presents two groups of signals clearly distinguished, similarly to Eu^{3+} and Sm^{3+}-doped nGCs. On one hand, the characteristic excitation peaks of Tb^{3+} ions from the ground state $^7F_6$ to the labelled excited levels in the 350-400 nm range. On the other hand, a group of more intense excitation peaks located at 248, 272 and 307 nm, which correspond to transitions from the $^8S_{7/2}$ ground level to the ^6D_J, ^6I_J and ^6P_J excited levels of Gd^{3+} ions, and points out the existence of ET from Gd^{3+} to Tb^{3+} ions. Fig. 8(a) also shows the emission spectrum exciting through the Gd^{3+} ions at 272 nm. Intense emissions from 480 to 650 nm can be observed, corresponding to transitions from the $^5D_4$ to ^7F_J (J=6,5,4,3) levels of Tb^{3+} ions, where 542 nm is dominant, yielding an intense green emission that is visible to the naked eye. Moreover, it should be noted that comparable emissions coming from the $^5D_3$ excited level to the ^7F_J (J=6,5,4,3,2) are also observed below 475 nm, which can be associated with low cross-relaxation (CR) processes between Tb^{3+} ions at this doping level [30,35] and low phonon frequency of $BaGdF_5$ nanocrystalline host [28].

Fig. 8.(b) shows the excitation spectrum of Dy^{3+}-doped nGCs, detecting at 597 nm, corresponding to $^4F_{9/2}\rightarrow{}^6H_{13/12}$ transition of Dy^{3+} ions. Direct excitation peaks assigned to transitions from ground $^6H_{15/2}$ level to excited levels $^4L_{19/2}$, $^4M_{15/2}$, $^6P_{7/2}$, $^4I_{11/2}$, $^4I_{13/2}$ and $^4F_{7/2}$ of Dy^{3+} ions are observed, along with much more intense excitation peaks of Gd^{3+}

ions at around 250 and 272 nm. These correspond to transitions from the $^8S_{7/2}$ ground state to ^6D_J, ^6I_J and ^6P_J excited levels, as it was previously analysed. The strong sensitization in Dy^{3+}-doped nGCs can be observed in Fig.8.(b), where the emission spectrum under indirect excitation through Gd^{3+} ions at 272 nm is presented. Four intense emission peaks (479, 573, 662 and 751 nm) that correspond to Dy^{3+} transitions appear along with the intense peak (311 nm) assigned to the $^6P_J \rightarrow {}^8F_{7/2}$ transition of Gd^{3+} ions.

The overall emitted colour for the studied nGCs can be represented by a point in the CIE standard chromaticity diagram [48]. The colour coordinates on this diagram correspond to the chromaticity seen by the naked eye after a correction to sensitive receptors of the eye. In this sense, Fig.9 (a) shows a possible tuneability as a function of the selected RE dopant ion, giving rise to a reddish-orange colour, with coordinates values of (0.53; 0.38) for Eu^{3+} or Sm^{3+}-doped nGCs. For Dy^{3+} (0.37; 0.40) and Tb^{3+}-doped (0.31; 0.42) nGCs, relatively closer values to equal energy white light illumination point (0.33; 0.33) are obtained. These results suggest that by adequate combination of these ions and doping level, this single-phased material might be a promising candidate for applications in UV-converting white LEDs.

Finally, in order to confirm the ET from Gd^{3+} to RE dopant ions, time-resolved luminescence measurements were carried out in the studied $BaGdF_5$ nGCs (see Fig. 9(b)). In all cases, luminescence decay was analysed by exciting the transition $^8S_{7/2} \rightarrow {}^6I_{7/2}$ (at 272 nm) and detecting the emission $^6P_{3/2} \rightarrow {}^8S_{7/2}$ (at 311 nm) of Gd^{3+} ions. The results were quantified in terms of effective lifetime $<\tau>$ obtained from the area under the curve through the expression $\tau_{eff} = \int_0^\infty I(t)dt/I(0)$. The obtained values indicate the luminescence decay lifetimes related with the studied transition. Thus, a value of 7.4 ms was obtained for the un-doped nGCs, while for the rest of the RE-doped nGCs, shorter lifetimes with values around 4.4 ms (Eu^{3+}, Sm^{3+} and Tb^{3+} ions) and 5.4 ms (Dy^{3+} ions) were obtained. These values can be related with the ET efficiency, through the expression $\eta_{ETE} = 1 - (\frac{\tau_{RE-doped}}{\tau_{un-doped)}})$, where $\tau_{\text{un-doped}}$ and $\tau_{\text{RE-doped}}$ are the effective lifetimes for the un-doped and RE-doped nGCs, respectively. All calculated values are included in the inset of Fig.9(b). showing similar efficiency values for Sm^{3+}, Eu^{3+} and Tb^{3+} ions, while a relatively lower one for Dy^{3+} ions is obtained, confirming in all cases the existence of an ET mechanism from the Gd^{3+} to the RE ions used as dopants.

4. Conclusions

RE (Eu^{3+}, Sm^{3+}, Tb^{3+} and Dy^{3+})-doped and un-doped nGCs comprising $BaGdF_5$ NCs were obtained under thermal treatment of precursor sol-gel glasses. By XRD, TEM-HRTEM and EDS measurements, the precipitation and distribution of 10 nm cubic sized $BaGdF_5$ NCs in the glass matrix was confirmed. Luminescent features of Eu^{3+} and Sm^{3+} ions, as probe ions, lead us to complete the structural analysis, confirming the distribution of a significant fraction of dopant ions into the fluoride nanocrystalline environment. In all cases, intense visible emissions were obtained through efficient energy transfer from Gd^{3+} to RE ions, suggesting that these materials can be considered as potential phosphor for colour converted UV LEDs.

Acknowledgments

The authors would like to thank Ministerio de Economía y Competitividad (MAT2014-57551-R (LUNALEDs) for financial support. We also would like to thank Mrs Julia Troyano for her valuable contribution and suggestions.

References

[1] R.-S. Liu, Phosphors, Up Conversion Nano Particles, Quantum Dots and Their Applications, Vol. 2, Springer, Taiwan, 2016.

[2] D. Chen, S. Liu, Z. Wan, Y. Chen, A highly sensitive upconverting nano-glass-ceramic-based optical thermometer, J. Alloys Compd. 672 (2016) 380-385.

[3] F. Zhang, Photon Upconversion Nanomaterials, Springer 2015.

[4] D. Chen, W. Xiang, X. Liang, J. Zhong, H. Yu, M. Ding, H. Lu, Z. Ji, Advances in transparent glass–ceramic phosphors for white light-emitting diodes- A review, J. of Eur. Ceram. Soc. 35 (2015) 859-869.

[5] L.X. Lovisa, V.D. Araújo, R.L. Tranquilin, E. Longo, M.S. Li, C.A. Paskocimas, M.R.D. Bomio, F.V. Motta, White photoluminescence emission from ZrO_2 co-doped with Eu^{3+}, Tb^{3+} and Tm^{3+}, J. Alloys Compd. 674 (2016) 245-251.

[6] X. Wang, T. Xu, P. Cai, T. Vu, H. J. Seo, Controlled synthesis, multicolor luminescence, and optical thermometer of bifunctional $NaYbF_4:Nd^{3+}@NaYF_4:Yb^{3+}$ active-core/active-shell colloidal nanoparticles, J. Alloys Compd. 691 (2017) 530-536.

[7] Y. Qin. Z. Hu, B. Han Lim, W. S. Chang, K. K. Chong, P. Zhang, H. Zhang, Sol-hydrothermal synthesis of $TiO_2:Sm^{3+}$ nanoparticles and their enhanced photovoltaic properties, J. Alloys Compd. 686 (2016) 803-809.

[8] W. Zhang, S. Ouyang, Z. Zhang, Y. Zhang, H. Xia, Luminescent properties of Eu^{3+}-doped glass ceramics containing $BaGdF_5$ nanocrystals under NUV-excitation for W-LEDs, Ceram. Intern. 41 (2015) 14035-14040.

[9] S.H. Lee, S.-R. Bae, Y.G. Choi, W. J. Chung, Eu^{2+}/Eu^{3+}-doped oxyfluoride glass ceramics with LaF_3 for white LED color conversion, Opt. Mater. 41 (2015) 71-74.

[10] W. Zhang, Y. Zhang, S. Ouyang, Z. Zhang, H. Xia, Enhanced luminescent properties of Sm^{3+} doped glass ceramics as potential red-orange phosphor for white light-emitting diodes, Mat. Lett. 160 (2015) 459-462.

[11] P. Dharmaiah, C.S.D. Viswanath, C. Basavapoornima, K.V. Krishnaiah, C.K. Jayasankar, S.-J. Hong, Luminescence and energy transfer in Dy^{3+}/Tb^{3+} co-doped transparent oxyfluorosilicate glass-ceramics for green emitting applications, Mater. Res. Bull. 83 (2016) 507-514.

[12] S. Ouyang, W. Zhang, Z. Zhang, Y.Zhang, Near-green-emitting Tb^{3+}-doped transparent glass ceramics containing Ba_2LaF_7 nanocrystals for application in white light-emitting diodes, J. Appl. Spectrosc. 83 (2016) 277-282.

[13] M. Kemere, J. Sperga, U. Rogulis, G. Krieke, J.Grube, Luminescence properties of Eu, RE^{3+} (RE = Dy, Sm, Tb) co-doped oxyfluoride glasses and glass–ceramics, J. Lumin. 181 (2017) 25-30.

[14] G. Sharma, R. Bagga, N. Mahendru, M. Falconieri, V. Gopal-Achanta, A. Goel, S. Nayab-Rasool, N. Vijaya, Influence of lead and cadmium fluoride variation on white light emission characteristics in oxyfluoride glasses and glass–ceramics, J. Lumin 159 (2015) 38-46.

[15] C. Zhu, D. Wu, J. Liu, M. Zhang, Y. Zhang, Color-tunable luminescence in Ce-, Dy-, and Eu-doped oxyfluoride aluminoborosilicate glasses, J. Lumin (in press) http://dx.doi.org/10.1016/j.jlumin.2016.11.004

[16] A.C. Yanes, J. del-Castillo, D. Luis, J. Puentes, Novel Sr_2LuF_7–SiO_2 nano-glass-ceramics: Structure and up-conversion luminescence, J. Lumin. 170 (2016) 789-794.

[17] H. K. Dan, D. Zhou, R. Wang, X. Yu, Q. Jiao, Z. Yang, Z. Song, J. Qiu, Energy transfer and upconversion emission of Er^{3+}/Tb^{3+}/Yb^{3+} co-doped transparent glass-ceramics containing Ba_2LaF_7 nanocrystals under heat treatment, Opt. Mater. 36 (2014) 639-644.

[18] J. del-Castillo, A.C. Yanes, S. Abe, P.F. Smet, Site selective spectroscopy in $BaYF_5$:RE^{3+} (RE=Eu,Sm) nano-glass–ceramics, J. Alloys Compd. 635 (2015) 136-141.

[19] A Santana-Alonso, AC Yanes, J Méndez-Ramos, J del-Castillo, VD Rodríguez, Down-shifting by energy transfer in Dy^{3+}–Tb^{3+} co-doped YF_3-based sol–gel nano-glass-ceramics for photovoltaic applications, Opt. Mater. 33 (2011) 587-591.

[20] J. del-Castillo, A.C. Yanes, A. Santana-Alonso, J Méndez-Ramos, Efficient dual-wavelength excitation of Tb^{3+} emission in rare-earth doped KYF_4 cubic nanocrystals dispersed in silica sol–gel matrix, Opt. Mater. 37 (2014) 511-515.

[21] J.J. Velázquez, V.D. Rodríguez, A.C. Yanes, J. del-Castillo, J. Méndez-Ramos, Photon down-shifting by energy transfer from Sm^{3+} to Eu^{3+} ions in sol-gel SiO_2-LaF_3 nano-glass-ceramics for photovoltaics, App. Phys. B. 108 (2012) 577-583.

[22] A.C. Yanes, J. del-Castillo, Enhanced emission via energy transfer in RE co-doped SiO_2-KYF_4 nano-glass-ceramics for white LEDs, J. Alloys Compd. 658 (2016) 170-176.

[23] M. Secu, C. E. Secu, Up-conversion luminescence of Er^{3+}/Yb^{3+} co-doped $LiYF_4$ nanocrystals in sol–gel derived oxyfluoride glass-ceramics, J. Non-Cryst. Solids 426 (2015) 78-82.

[24] D. Chen, S. Liu, Z. Wan, Z. Ji, Light manipulation in upconverting nano-glass-ceramics via Ce^{3+} doping, Journal of Eur. Ceram. Soc. 36 (2016) 1841-1845.

[25] T. Grzyb, M. Runowski, S. Lis, Facile synthesis, structural and spectroscopic properties of GdF_3:Ce^{3+}, Ln^{3+} (Ln^{3+}=Sm^{3+},Eu^{3+},Tb^{3+},Dy^{3+}) nanocrystals with bright multicolor luminescence, J. Lumin. 154 (2014) 479-486.

[26] X. Zhang, Y. Chen, L. Zhou, Q. Pang, M. Gong, Synthesis of a Broad-Band Excited and Multicolor Tunable Phosphor Gd_2SiO_5:Ce^{3+},Tb^{3+},Eu^{3+} for Near-Ultraviolet Light-Emitting Diodes, Ind. Eng. Chem. Res. 53 (2014) 6694-6698.

[27] H. Guan, Y. Song, K. Zheng, Y. Sheng, H. Zou, $BaGdF_5$: Dy^{3+}, Tb^{3+}, Eu^{3+} multifunctional nanospheres: paramagnetic, luminescence, energy transfer, and tunable color, Phys. Chem. Chem. Phys. 18 (2016) 13861-13873.

[28] L. Guo, Y. Wang, Y. Wang, J. Zhang, P. Dong, Crystal structure and up- and down-conversion properties of Yb^{3+}, Ho^{3+} codoped $BaGdF_5$ solid-solution with different morphologies, Cryst. Eng. Comm. 14 (2012) 3131-3141.

[29] D. Yang, C. Li, G. Li, M. Shang, X. Kang, J. Lin, Colloidal synthesis and remarkable enhancement of the up-conversion luminescence of $BaGdF_5$:Yb^{3+}/Er^{3+} nanoparticles by active-shell modification, J. Mat. Chem. 21 (2011) 5923-5927.

[30] Y. Zhang, J. Lv, N. Ding, S. Jiang, T. Zheng, J. Li, Tunable luminescence and energy transfer from Gd^{3+} to Tb^{3+} ions in silicate oxyfluoride scintillating glasses via varying Tb^{3+} concentration, J. Non-Cryst. Solids 423-424 (2015) 30–34.

[31] Q. Shi, F. You, D. Xie, H. Peng, Y. Huang, Y. Tao, S. Huang, Efficient energy transfer from the Pr^{3+} 4f5d states to Eu^{3+} via Gd^{3+} in K_2GdF_5, J. Lumin. 145 (2014) 620-625.

[32] B. Szpikowska, N. Pawlik, A. S. Swinarew, Luminescence of Eu^{3+}/Gd^{3+} co-doped silicate sol–gel powders, J Lumin. 166 (2015) 356-360.

[33] Q. Wang, S. Ouyang, W. Zhang, B. Yang, Y. Zhang, H. Xia, Luminescent properties of Ce^{3+}-doped transparent oxyfluoride glass ceramics containing $BaGdF_5$ nanocrystals, J. of Rare-Earths 33 (2015) 13-19.

[34] K. Biswas, S. Balaji, P. Karmakar, K. Annapurna, Formation and spectral probing of transparent oxyfluoride glass-ceramics containing (Eu^{2+},Eu^{3+}:$BaGdF_5$) nano-crystals, Opt. Mater. 39 (2015) 153-159.

[35] S. Huang, M. Gu, Enhanced luminescent properties of Tb^{3+} ions in transparent glass ceramics containing $BaGdF_5$ nanocrystals, J. Non-Cryst. Solids 358 (2012) 77-80.

[36] B. Yang, Q. Wang, W. Zhang, S. Ouyang, Y. Zhang, Luminescent properties of Tb^{3+}-doped transparent glass ceramics, J. Lumin. 158 (2015) 390-395.

[37] G. Lee, N. Savage, B. Wagner, Y. Zhang, B. Jacobs, H. Menkara, C. Summers, Z. Kang, Synthesis and luminescence properties of transparent nanocrystalline GdF_3:Tb glass-ceramic scintillator, J. Lumin. 147 (2014) 363-366.

[38] B. Szpikowska-Sroka, L. Żur, R. Czoik, T. Goryczka, M. Żądło, W. A. Pisarski, Ultraviolet-to-visible downconversion luminescence in sol gel oxyfluoride glass ceramics containing Eu^{3+}:GdF_3 nanocrystals, Opt. Lett. 11 (2014) 3181-3184.

[39] C.J. Brinker, G.W. Scherer, Sol–Gel Science: The Physics and Chemistry of Sol-Gel Processing, Academic Press, Boston 1990.

[40] A. Biswas, G. S. Maciel, C. S. Friend and P. N. Prasad, Upconversion properties of a transparent Er^{3+}-Yb^{3+} co-doped LaF_3–SiO_2 glass-ceramics prepared by sol-gel method, J. Non-Cryst. Solids 316 (2003) 393-397.

[41] J. Rodríguez-Carvajal, Recent advances in magnetic structure determination by neutron powder diffraction, Phys. B 192 (1993) 55-60.

[42] L. Lei, D. Chen, F. Huang, Y. Yu, Y. Wang, Syntheses and optical properties of monodisperse $BaLnF_5$ (Ln=La–Lu,Y) nanocrystals, J. Alloys Compd. 540 (2012) 27-31.

[43] C. Xu, M. Ma, L. Yang, S. Zeng, Q. Yang, Upconversion luminescence and magnetic properties of ligand-free monodisperse lanthanide doped $BaGdF_5$ nanocrystals, J. Lumin. 131 (2011) 3544-2549.

[44] P. Karmakar, A. K. Subudhi, K. Biswas, K. Annapurna, Crystallization kinetics analysis of BaF_2 and $BaGdF_5$ nanocrystals precipitated from oxyfluoride glass systems: A comparative study, Termochem. Acta 610 (2015) 1-9.

[45] Q. Wang, W. Zhang, S. Ouyang, Y. Zhang, H. Xia, Luminescent properties of Ce^{3+} ion and Tb^{3+} ion co-doped transparent oxyfluoride glass ceramics containing $BaGdF_5$ nanocrystals, J. Non-Cryst. Solids 411 (2015) 35-39.

[46] B. Karmakar, K. Rademann, A. L. Stepanov, Glass Nanocomposites: Synthesis, Properties and Applications, Chapter 2, pp. 93, Elsevier, 2016.

[47] K. Binnenmans, Interpretation of europium (III) spectra, Coord. Chem. Rev. 295 (2015) 1-45.

[48] CIE, International Commission on Illumination, Colorimetry: Official Recommendations of the International Commission on Illumination, Publication CIE no. 15 (E-1.3.1), Bureau Central de la CIE, Paris, 1971

Figure Captions

Fig.1. XRD patterns of un-doped and Eu^{3+}-doped nGCs heat-treated at 650 ºC. XRD pattern of a precursor sol-gel glass and standard peaks of $BaGdF_5$ (JCPDS 24-0098) are also included for comparison.

Fig.2. EDS analysis of Eu^{3+}-doped nGC (a) from glass matrix and (b) an area containing glass matrix with several $BaGdF_5$ NCs.

Fig.3 (a) TEM and (b) HRTEM images of Eu^{3+}-doped nGC. Insets show power spectrum (FFT pattern) and filtered higher-contrasted image of red and blue squared nanoparticles.

Fig.4. Excitation and emission spectra of un-doped nGC, detecting and exciting at indicated wavelengths. Energy level diagram of Gd^{3+} ions is also included.

Fig.5. Energy level diagrams of Gd^{3+} and RE ions (RE=Eu^{3+}, Sm^{3+}, Dy^{3+} and Tb^{3+}), showing main excitation and emission transitions (up and down solid arrows) and proposed ET mechanisms (dashed arrows).

Fig.6 (a) Excitation spectrum of Eu^{3+}-doped nGC, detecting at 593 nm ($^5D_0 \rightarrow {}^7F_1$ transition of Eu^{3+} ions). (b) Corresponding emission spectra obtained through Eu^{3+} ions excitation

(393 and 464 nm) and indirect excitation through Gd^{3+} ions (272 nm). Emission spectrum of SiO_2:Eu^{3+} glass exciting at 393 nm is also included for comparison.

Fig.7. (a) Excitation spectrum of Sm^{3+}-doped nGC, detecting at 597 nm ($^4G_{5/2}\rightarrow{}^6H_{7/2}$ transition of Sm^{3+} ions). (b) Corresponding emission spectra exciting at indicated wavelengths. An emission spectrum of a SiO_2 glass doped with Sm^{3+}, exciting at 398 nm has been included for comparison. Emission spectra have been normalized at $^4G_{5/2}\rightarrow{}^6H_{7/2}$ transition of Sm^{3+} ions.

Fig.8 (a) Emission spectrum of Tb^{3+}-doped nGC, detecting at 543 nm($^5D_4\rightarrow{}^7F_5$ transition of Tb^{3+} ions). Corresponding excitation spectrum, exciting at 272 nm (see inset). Spectra have been normalized at $^5D_4\rightarrow{}^7F_5$ transition of Tb^{+} ions. (b) Emission spectrum of Dy^{3+}-doped nGC, detecting at 597 nm ($^4F_{9/2}\rightarrow{}^6H_{13/12}$ transition of Dy^{3+} ions). (b) Corresponding excitation spectrum exciting at 272 nm (see inset).

Fig.9 (a) Color coordinates in the CIE standard chromaticity diagram of RE-doped nGCs, under 272 nm excitation. (b) Effective lifetime blues of nGCs with composition $95SiO_2$-$5BaGdF_5$, un-doped or doped with the indicated RE ions.

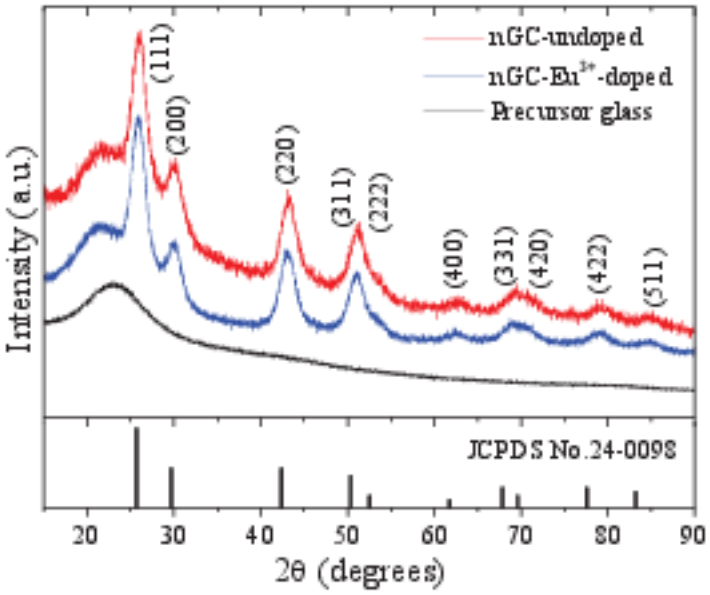
nGC-undoped
nGC-Eu3+-doped
Precursor glass
(111)
(200)
(220)
(311)
(222)
(400)
(331)
(420)
(422)
(511)
Intensity (a.u.)
JCPDS No.24-0098
20
30
40
50
60
70
80
90
2θ (degrees)

Fig.1.

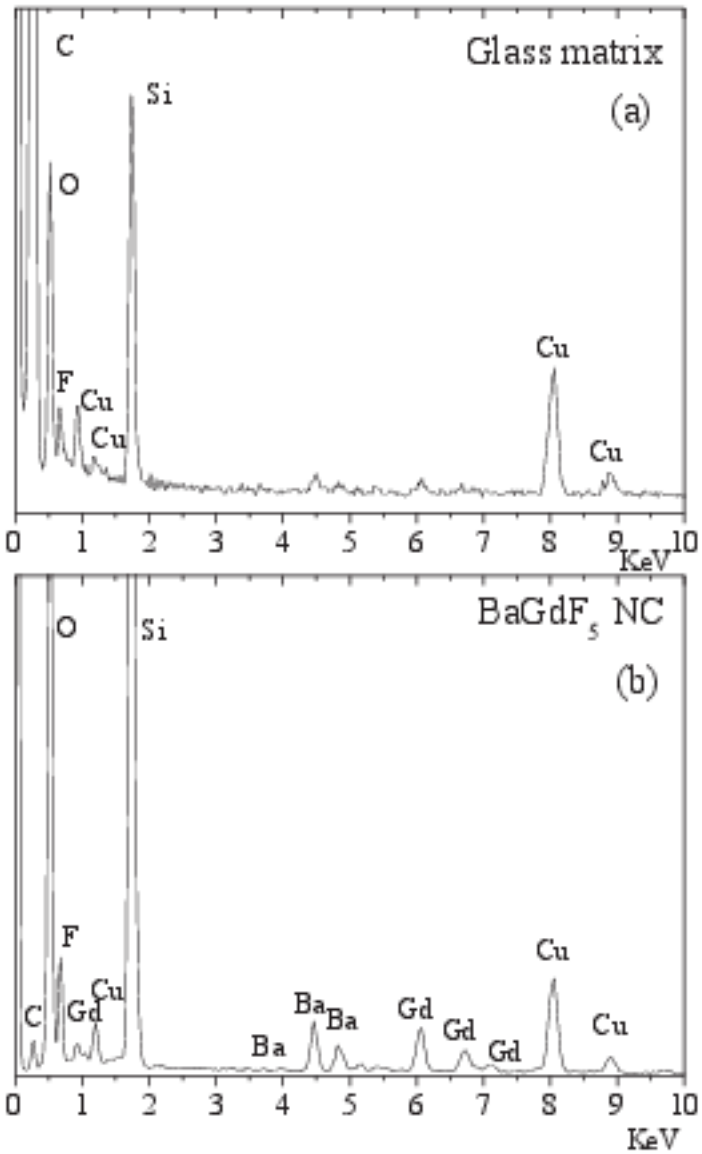
C
Glass matrix
Si
(a)
O
F
Cu
Cu
Cu
Cu
0 1 2 3 4 5 6 7 8 9 10
KeV
O
Si
BaGdF5 NC
(b)
F
Cu
C
Gd
Ba
Ba
Ba
Gd
Gd
Gd
Cu
Cu
0 1 2 3 4 5 6 7 8 9 10
KeV

Fig.2.

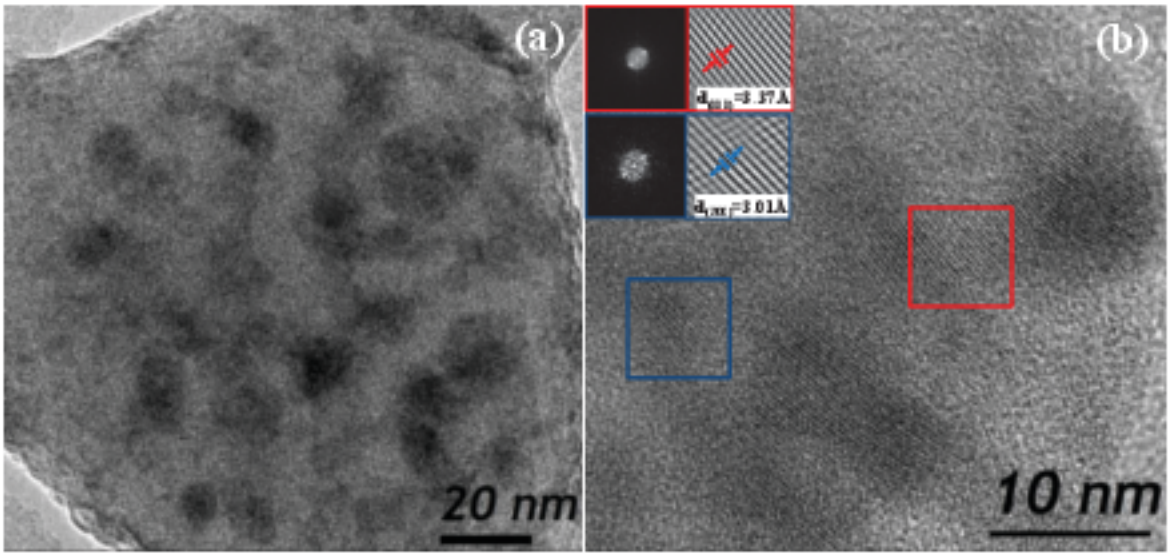

Fig.3

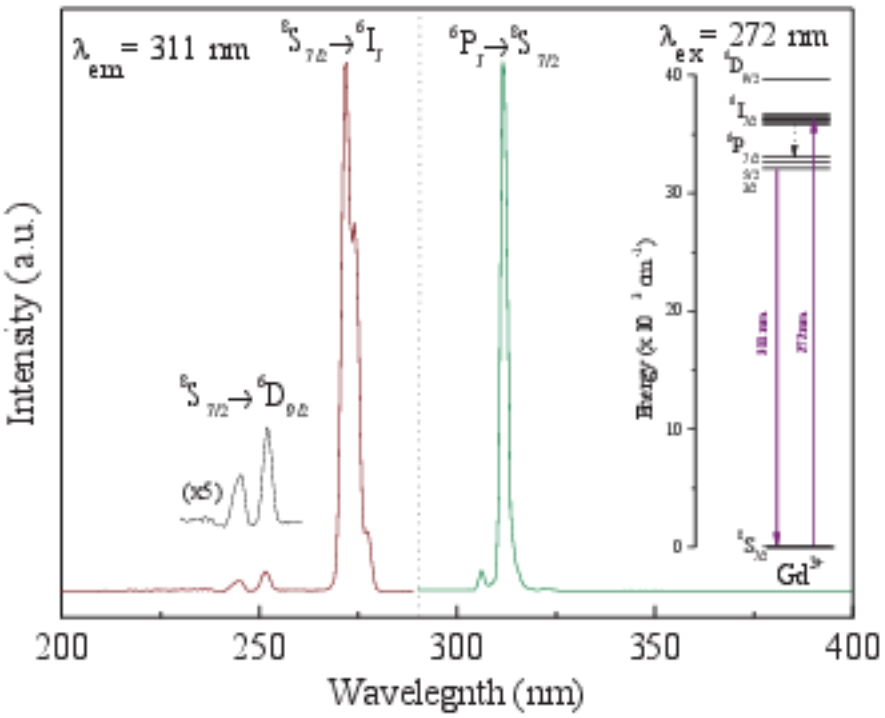
λem = 311 nm
8S7/2→6IJ
6PJ→8S7/2
λex = 272 nm
8S7/2→6D9/2
(x5)
Intensity (a.u.)
Wavelegnth (nm)
200
250
300
350
400
Energy (x 10^3 cm^-1)
0
10
20
30
40
6D9/2
6I7/2
6P7/2
5/2
3/2
8S7/2
Gd3+

Fig.4.

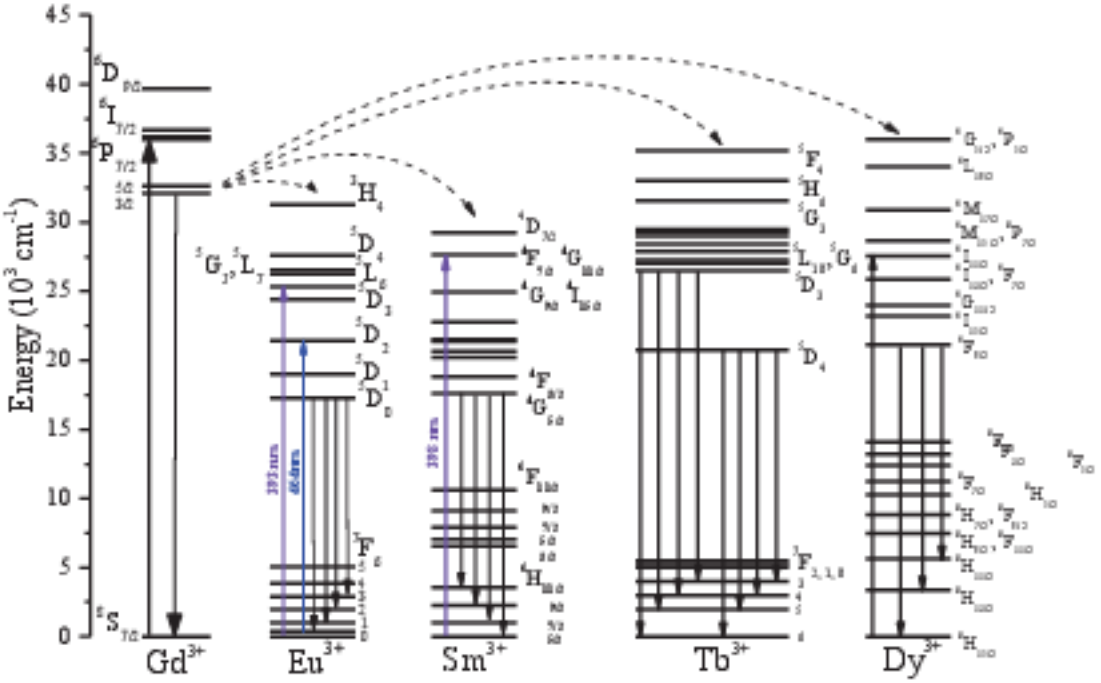

Fig.5

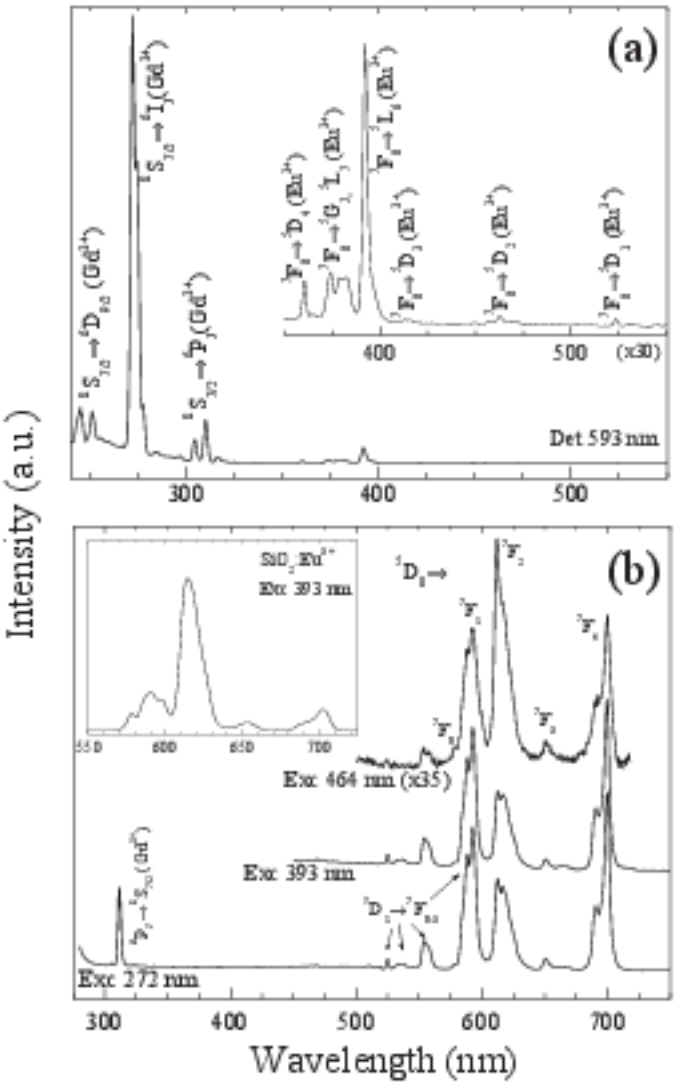
(a)
Det 593 nm
(x30)
(b)
Exc 464 nm (x35)
Exc 393 nm
Exc 272 nm
Intensity (a.u.)
Wavelength (nm)

Fig.6.

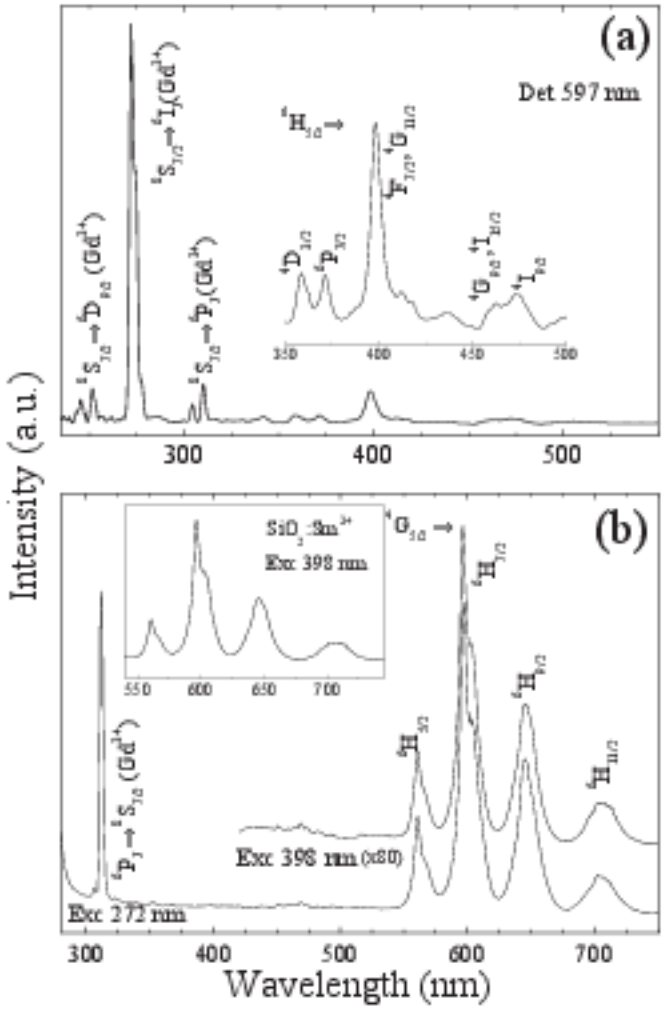
(a)
Det 597 nm
$^8S_{7/2} \rightarrow {}^6D_{9/2}$ (Gd^{3+})
$^8S_{7/2} \rightarrow {}^6I_J$($Gd^{3+}$)
$^8S_{7/2} \rightarrow {}^6P_J$($Gd^{3+}$)
$^6H_{7/2} \rightarrow$
$^6D_{3/2}$
$^6P_{7/2}$
$^6F_{7/2}$, $^6G_{11/2}$
$^6G_{9/2}$, $^6I_{11/2}$
$^6I_{9/2}$
350
400
450
500
300
400
500
(b)
SiO_2:Sm^{3+}
Exc 398 nm
550
600
650
700
$^6G_{7/2} \rightarrow$
$^6H_{7/2}$
$^6H_{9/2}$
$^6H_{11/2}$
$^6H_{5/2}$
$^6P_J \rightarrow {}^8S_{7/2}$ (Gd^{3+})
Exc 398 nm (x80)
Exc 272 nm
300
400
500
600
700
Intensity (a.u.)
Wavelength (nm)

Fig.7

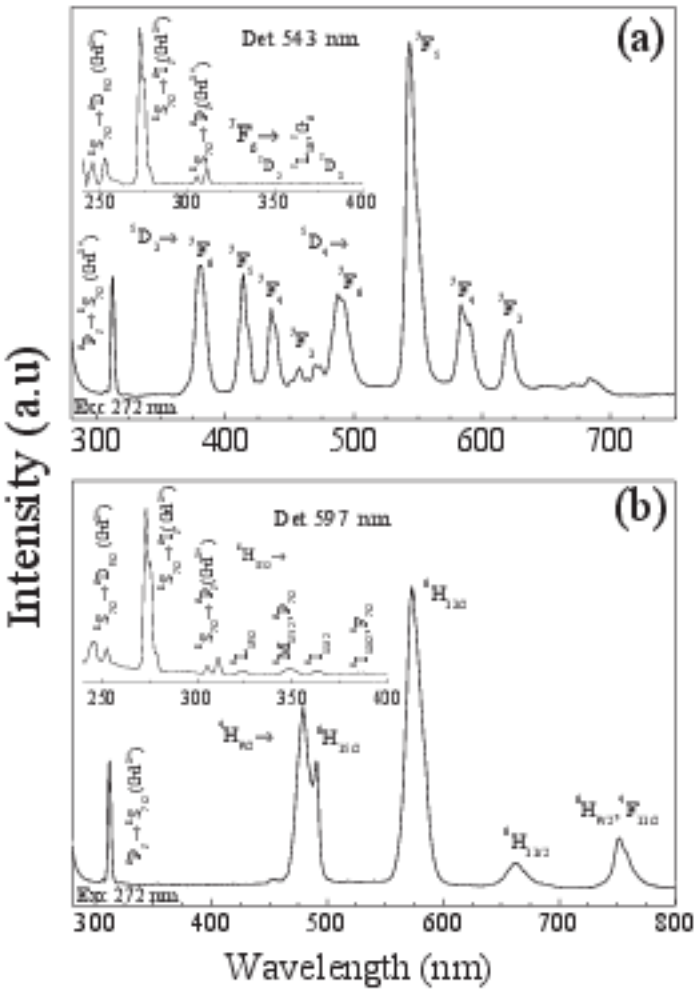
(a)
Det 543 nm
Exc 272 nm
(b)
Det 597 nm
Exc 272 nm
Intensity (a.u)
Wavelength (nm)
300
400
500
600
700
800
250
300
350
400

Fig.8

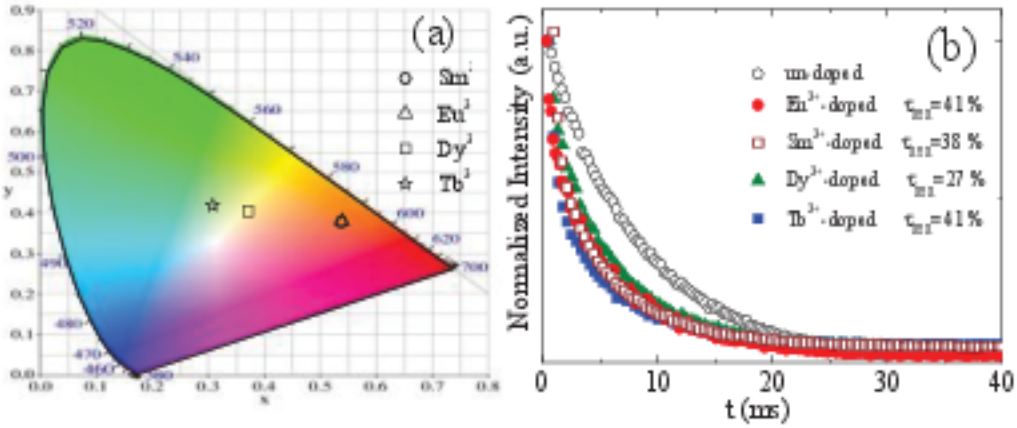
(a)
Sm
Eu
Dy
Tb
x
y
(b)
un-doped
Eu3+-doped τ1/e=41 %
Sm3+-doped τ1/e=38 %
Dy3+-doped τ1/e=27 %
Tb3+-doped τ1/e=41 %
Normalized Intensity (a.u.)
t (ms)
0
10
20
30
40

Fig.9

Journal of Alloys and Compounds:" **Bright luminescence of Gd^{3+} sensitized RE^{3+}-doped SiO_2-$BaGdF_5$ glass-ceramics for UV-LEDs color conversion"**

- We obtained un-doped and RE doped glass-ceramics with cubic $BaGdF_5$ nanocrystals
- XRD, TEM and EDAX confirm the precipitation and distribution of $BaGdF_5$ nanocrystals
- Intense visible emissions by energy transfer from Gd^{3+} to RE^{3+} ions were obtained
- This material can be considered as potential phosphor for colour converted UV LEDs